

# Ionic Highways from Covalent Assembly in Highly Conducting and Stable Anion Exchange Membrane Fuel Cells

Yoonseob Kim,<sup>†,‡,§</sup> Yanming Wang,<sup>§,⊥</sup> Arthur France-Lanord,<sup>§,⊥</sup> Yichong Wang,<sup>†</sup>  
You-Chi Mason Wu,<sup>†,§</sup> Sibö Lin,<sup>†,§</sup> Yifan Li,<sup>†</sup> Jeffrey C. Grossman,<sup>\*,§,§</sup> and Timothy M. Swager<sup>\*,†,§</sup>

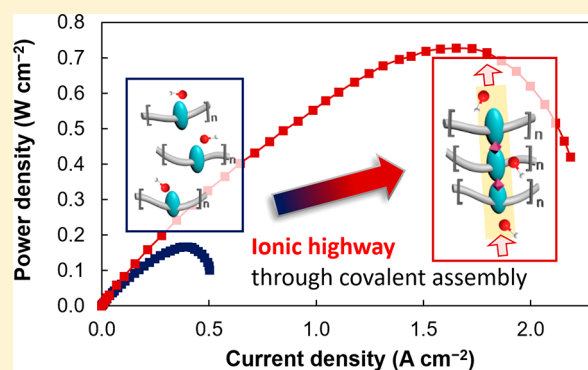
<sup>†</sup>Department of Chemistry, Massachusetts Institute of Technology, Cambridge, Massachusetts 02139, United States

<sup>‡</sup>Department of Chemical and Biological Engineering, Hong Kong University of Science and Technology, Clear Water Bay, Kowloon, Hong Kong SAR, China

<sup>§</sup>Department of Materials Science and Engineering, Massachusetts Institute of Technology, Cambridge, Massachusetts 02139, United States

## Supporting Information

**ABSTRACT:** A major challenge in the development of anion exchange membranes for fuel cells is the design and synthesis of highly stable (chemically and mechanically) conducting membranes. Membranes that can endure highly alkaline environments while rapidly transporting hydroxides are desired. Herein, we present a design using cross-linked polymer membranes containing *ionic highways* along charge-delocalized pyrazolium cations and homoconjugated triptycenes. These ionic highway membranes show improved performance. Specifically, a conductivity of 111.6 mS cm<sup>-1</sup> at 80 °C was obtained with a low 7.9% water uptake and 0.91 mmol g<sup>-1</sup> ion exchange capacity. In contrast to existing materials, ionic highways produce higher conductivities at reduced hydration and ionic exchange capacities. The membranes retain more than 75% of their initial conductivity after 30 days of an alkaline stability test. The formation of ionic highways for ion transport is confirmed by density functional theory and Monte Carlo studies. A single cell with platinum metal catalysts at 80 °C showed a high peak density of 0.73 W cm<sup>-2</sup> (0.45 W cm<sup>-2</sup> from a silver-based cathode) and stable performance throughout 400 h tests.



Advances in fuel cell technologies over recent decades have enabled the production of fuel cell vehicles by major automobile manufacturers.<sup>1</sup> The advantages of fuel cell vehicles include environmental friendliness, convenient/rapid refueling, compatibility with current fossil fuel infrastructure, and the ability to run long range on a single fueling. Current commercial vehicles use proton exchange membrane fuel cells, and the high power output is the result of efficient platinum-catalyzed reactions and fast ion exchange through fluorocarbon membranes such as Nafion.<sup>2</sup> However, these systems are expensive from both the membrane and catalyst standpoint, which is hindering broader adoption of this technology.<sup>1</sup> Recently, anion exchange membrane based fuel cells (AEMFCs) that use cationic polymeric hydroxide-conducting membranes as separators have gained interest because they function with less expensive metal catalysts.<sup>3–7</sup> To realize this potential, AEMs must address three major issues. First, fuel cells often operate in a nearly 100% humidity level, which causes high water uptake and swelling of the charged polymer membranes. Excessive swelling causes instabilities and loss of performance,<sup>8</sup> and freestanding membranes need to limit dimensional changes. Second, hydroxide, a strong base and nucleophile, degrades most cationic organic membranes at

60–80 °C operating temperatures.<sup>9</sup> Avoiding degradation is necessary for stable, long-term operation of the fuel cells. Finally, the hydroxide conductivity must be high (>100 mS cm<sup>-1</sup>) to meet the desired power output to drive an automotive motor. The design of stable cationic polymer networks for fast anion transport is best solved by chemical principles.<sup>10</sup> There has been progress on these fronts with the incorporation of cross-linked networks to prevent swelling,<sup>11,12</sup> ether-free networks to impart improved chemical stability,<sup>7,9</sup> and increasing the ion exchange capacity (IEC) to achieve higher conductivity.<sup>13,14</sup> However, in most cases, these solutions require trade-offs in properties. For example, cross-linking of hydrocarbon backbones can present challenges and can give reduced IEC. Similarly, increasing IEC often results in increased water uptake and polymer swelling. Designs that address all three AEM criteria simultaneously without compromises are rare.

Herein, we report highly conducting AEMs that are mechanically and chemically stable. Starting with a high free

Received: August 13, 2019

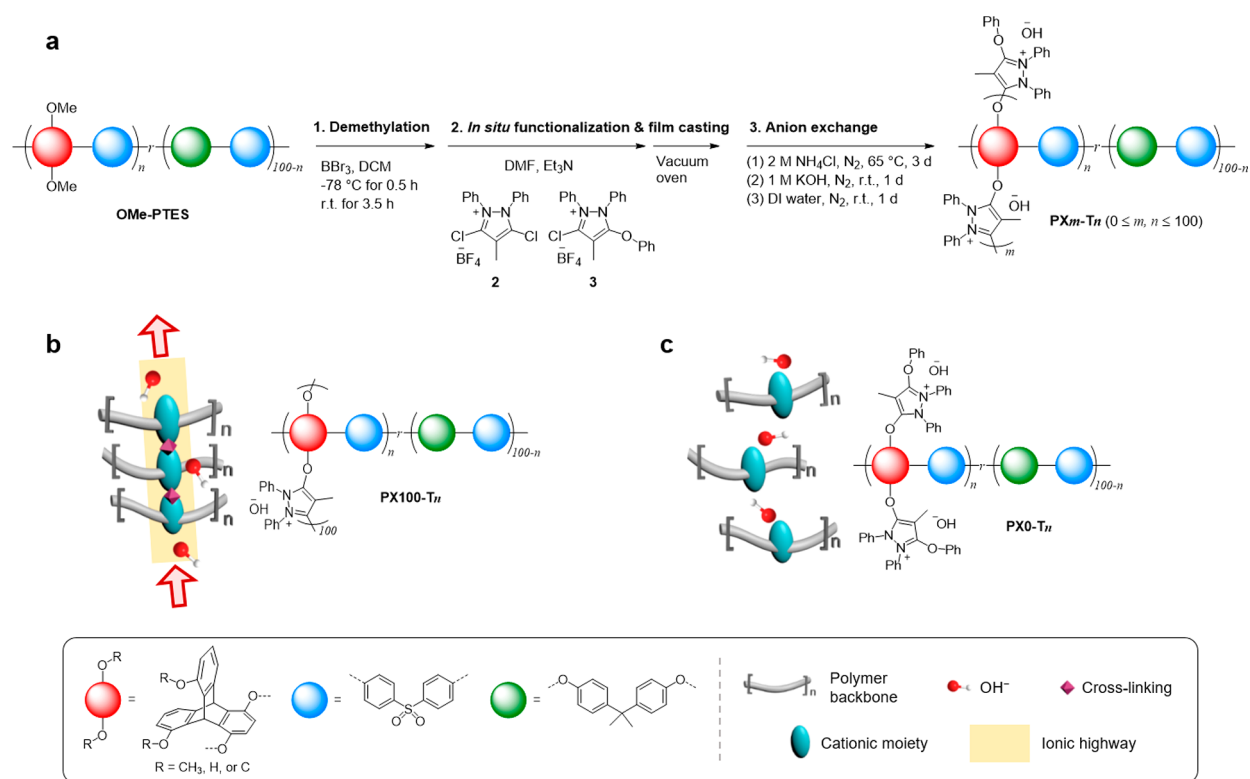


**Figure 1.** Design of ionic highway through a pyrazolium cross-linked triptycene polymer. (a) Schematic of conversion from poly(methoxy-triptycene ether sulfone) (OMe-PTES) to pyrazolium cross-linked poly(triptycene ether sulfone) (PX $m$ -T $n$ ) via demethylation, *in situ* functionalization and film casting, and anion exchange. (b) Schematic for a case of 100% degree of cross-linking. Anion transport is facilitated through delocalized cationic charges of pyrazoliums over triptycene and homoconjugation in the triptycene. (c) Schematic for a case of 0% degree of cross-linking. Anions would face much higher activation energy for transport. See Figures S7 and S8 for comprehensive schemes of chemical structures.

volume poly(hydroxy-triptycene ether sulfone) scaffold, cationic pyrazolium groups are introduced as covalently bound cross-linkers and pendant groups by a reaction with dichloro- and monochloro-pyrazolium ions. A series of pyrazolium cross-linked poly(triptycene ether sulfone)s were studied (PX $m$ -T $n$ ;  $0 \leq m, n \leq 100$ ,  $m$  denotes the intended percent of cross-linking, and  $n$  denotes the percent of triptycene repeats in the polymer, Figure 1). Reactions with the dichloro-pyrazolium cause cross-links, and addition of monochloro-pyrazolium gives pendant cations. The cross-linking was optimized for mechanical properties, and the *ionic highways* (Figure 1b) form as a combination of delocalized pyrazolium cations that are organized and homoconjugated by connection to triptycenes.<sup>15</sup> We demonstrate the utility of these AEMs containing ionic highways in hydroxide ion conducting fuel cells and show sustained high power output.

## INTRODUCING IONIC HIGHWAYS IN AN ANION EXCHANGE MEMBRANE

At the onset of this study, we set three design criteria, each addressing the challenges mentioned above, under a theme of creating an ionic highway. First, we needed to prevent high water uptake and swelling by constructing a cross-linked polymer network.<sup>11,12</sup> We decided installing cations as the cross-linkers would be the preferred strategy, as it balances IEC and mechanical stability. Second, we targeted fully substituted cationic rings to avoid reactive C–H groups. Experimental<sup>16</sup> and theoretical<sup>17</sup> studies have shown that deprotonation of the cation rings is a major degradation mechanism, and fully

substituted ring structures have improved alkaline stability.<sup>18</sup> Third, we expected that the covalent assembly of repeating ionic segments—*ionic highway*—would result in higher conductivity by lowering the activation barriers for ion transport.<sup>19</sup> These collective efforts created repeating segments of pyrazolium cations and triptycenes, where homoconjugation to the triptycenes helped to further delocalize the cationic charge of the ionic highway (Figure 1).

Charge delocalization of cations is an established way to reduce reactivity with nucleophilic and basic hydroxide anions. Resonance stabilization can enhance cations' alkaline stability as can be seen even in cases of guanidiniums, imidazoliums, and pyridiniums,<sup>16,18,20</sup> although we note that fully substituted and sterically hindered benzimidoliums and aminophosphonium cations go into a top rank for alkaline stability.<sup>21</sup> In this study, we expand the cationic groups in AEMs to include pyrazolium groups with additional  $\pi$  donors. These are aromatic resonance-stabilized cations that can be conveniently incorporated as cross-linkers or pendants.<sup>22</sup> Although there are considerable efforts in creating high-performing AEMs through microscale phase segregation,<sup>23,24</sup> previous investigations have not pursued covalent assembly of repeating ionic cross-links to facilitate hydroxide transport.

## DESIGNING MONOMERS AND POLYMERS AND *IN SITU* MEMBRANE PREPARATIONS

We have introduced stable cationic rings, generated from 3,5-dichloropyrazolium, in AEMs. Our efforts were guided by density functional theory (DFT) calculations of the  $\text{pK}_a$  value

of the proton at the alpha methyl of 4-methyl-3,5-diphenoxy-1,2-diphenyl-pyrazolium tetrafluoroborate (**4**) and the alpha methylene of 4-butyl-3,5-diphenoxy-1,2-diphenyl-pyrazolium tetrafluoroborate (**7**).<sup>17</sup> These calculations reveal that these  $pK_a$ 's for **4** and **7** are 39.9 and 47.0, respectively (Figures S9d, S10d, and Note S2), and both represent particularly high values for organic cations.<sup>17</sup> The five-membered cationic dichloro-alkyl-diphenyl pyrazolium tetrafluoroborates were synthesized by adaptation of literature procedures<sup>22,25</sup> (Figures S1 and S4). Two-step procedures from commercial materials resulted in 4-methyl-3,5-dichloro-1,2-diphenyl-pyrazolium tetrafluoroborate (**2**) and 4-butyl-3,5-dichloro-1,2-diphenyl-pyrazolium tetrafluoroborate (**6**) with high overall yields (>72%). The cationic nature of these intermediates makes them excellent substrates for nucleophilic aromatic substitution of the chlorides with oxygen- or nitrogen-based nucleophiles. Reactions with phenol result in **4** and **7** which were used for alkaline stability tests (Figures S3 and S5). The  $\pi$ -electron-donating phenoxy groups provide additional stabilization of the cationic pyrazolium groups. For the simplest substituted pyrazolium, at least four different resonance structures can be drawn with all atoms in a preferred octet resonance structure (Figure S11).

The alkaline stability of **4** and **7** was tested by *in situ* NMR monitoring solutions at 1, 2, and 5 M KOH solutions in CD<sub>3</sub>OH at 80 °C using an internal standard.<sup>16</sup> Periodically, the solutions were analyzed by <sup>1</sup>H NMR spectroscopy to determine key cation signals relative to an internal standard. This set of tests showed high stability of **4** and **7** under alkaline conditions, and more than 91, 85, and 82% of the **4** and 93, 88, and 84% of the **7** persisted after heating at 80 °C in 1, 2, and 5 M KOH solutions over 30 days (Figures 2 and S9a–c). It

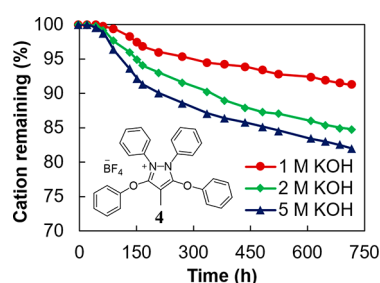


**Figure 2.** Long-term alkaline stability of **4** at 80 °C. Percent remaining of **4** in 1, 2, and 5 M KOH solutions in CD<sub>3</sub>OH at 80 °C, determined by <sup>1</sup>H NMR spectroscopy relative to an internal standard. See Figure S9 for the time-tracking NMR data.

should be emphasized that the NMR spectra remained relatively clean, except the small peaks at 7.51 and 7.83 ppm from cleavage of C–O bonds. Although **7** showed slightly higher alkaline stability (Figure S10a–c,e), we decided to use the methyl pyrazolium, **4**, for further studies. Specifically, we anticipate more thermal mobility with butyl pyrazolium (the melting temperatures of **4** and **7** are 216–218 and 148–150 °C, respectively) and potentially lower conductivity with longer butyl chains.<sup>26</sup> We synthesized 4-methyl-3-chloro-5-phenoxy-1,2-diphenyl-pyrazolium tetrafluoroborate (**3**, Figure S2), which can be used to graft cations onto polymers without introducing cross-linking that occurs by reaction with dichloropyrazolium (**2**). Hence, by simply changing the ratio between **2** and **3**, we can change  $m$  values in the membrane. Additionally, **3** adds one cation for every reactive hydroxyl

on the polymer, wherein **2** adds one cation for every two reactive hydroxyls. Hence, the ratio of these reactants also controls the IEC.

As a core polymer structure, we focused on triptycene-containing poly(ether sulfone), which has been previously shown to produce molecularly defined porosity (free volume) and facilitated ion transport while promoting solubility and enhancing mechanical properties.<sup>27,28</sup> In this case, we introduced modified triptycenes that can present a free hydroxyl group on each pendant benzene ring. This structure enables attachment of pyrazolium groups by nucleophilic substitution as pendants or as a cross-linking group (Figure 1). The proximate nature of the hydroxyl groups is key to the creation of the ionic highway. The polymer synthesis begins with 1,8-dimethoxy-benzanthracene-13,16-dione (**10**, Figure S6), wherein the hydroxyls are protected as methoxy groups.<sup>29,30</sup> Monomer **10** was synthesized in three steps from commercially available and low-cost 1,8-dihydroxyanthraquinone with a high overall yield of 73%. Copolymers were synthesized using **10**, with bisphenol A and bis(4-fluorophenyl) sulfone, via nucleophilic aromatic substitution ( $S_NAr$ ), with K<sub>2</sub>CO<sub>3</sub> as a base and dimethylacetamide as a solvent (Figure S7). Bisphenol A was introduced to lower  $T_g$  of the resulting polymer for increased film compliance. The  $S_NAr$  reaction produced high molecular weight poly(methoxy-triptycene ether sulfone), OMe-PTES ( $n = 50$ ;  $M_n$ : 107 kDa,  $M_w$ : 250 kDa, and PDI: 2.33) (Figure S12; molecular weight information on polymer of  $n = 75$  is also included). Subsequently, the OMe-PTES was quantitatively demethylated (<sup>1</sup>H NMR, Figure S7) by reaction with BBr<sub>3</sub> at –78 °C to yield poly(hydroxy-triptycene ether sulfone) (OH-PTES).

We fabricated membranes by *in situ* reactions of OH-PTES ( $n = 50$ , **12**) and pyrazolium dichloride (**2**) and monochloride (**3**) during film casting from dimethylformamide/triethylamine solution (Figure S8). By simply changing the amount of each **2** and **3** added, we produced three pyrazolium cross-linked poly(triptycene ether sulfone) membranes with different  $m$ , PX75-T50, PX40-T50, and PX10-T50 (Table S1, Figure S13, and Figure S14 for solid-state NMR spectra of membranes). The substitution reaction between hydroxy on the polymer and chlorides of **2** and **3** resulted in quantitative loss of chlorides as determined by energy-dispersive X-ray spectroscopy, and the final membranes were subjected to ion exchange of BF<sub>4</sub><sup>–</sup> to OH<sup>–</sup> (Figure S15). We found that polymers with  $n$  of equal to or greater than 63 result in too brittle of freestanding membranes. Also, for  $n = 50$ , 100% and 0% cross-linking did not result in freestanding membranes (Tables S1 and S2). Within these restrictions, we studied three membranes, PX75-T50, PX40-T50, and PX10-T50, that showed a good balance of material properties (Figures 1 and 3). Membranes prepared via slow drying in a vacuum oven have uniform thickness:  $53 \pm 4$ ,  $55 \pm 3$ , and  $64 \pm 5$   $\mu$ m for PX75-T50, PX40-T50, and PX10-T50, respectively (Figure S13). Our *in situ* preparation method has distinct advantages and allows simultaneous functionalization and cross-linking to tune the polymer's properties. The cross-linked freestanding membranes showed satisfactory mechanical properties (Figure S16) with sufficiently high Young's moduli (172 and 117 MPa for PX75-T50 and PX10-T50, respectively) and ultimate tensile strengths (264 and 144 MPa for PX75-T50 and PX10-T50, respectively). Hence, these materials were robust enough for fuel cell testing wherein they must be compressed without fracturing under the pressure of high-torque bolts (5.5 N m).



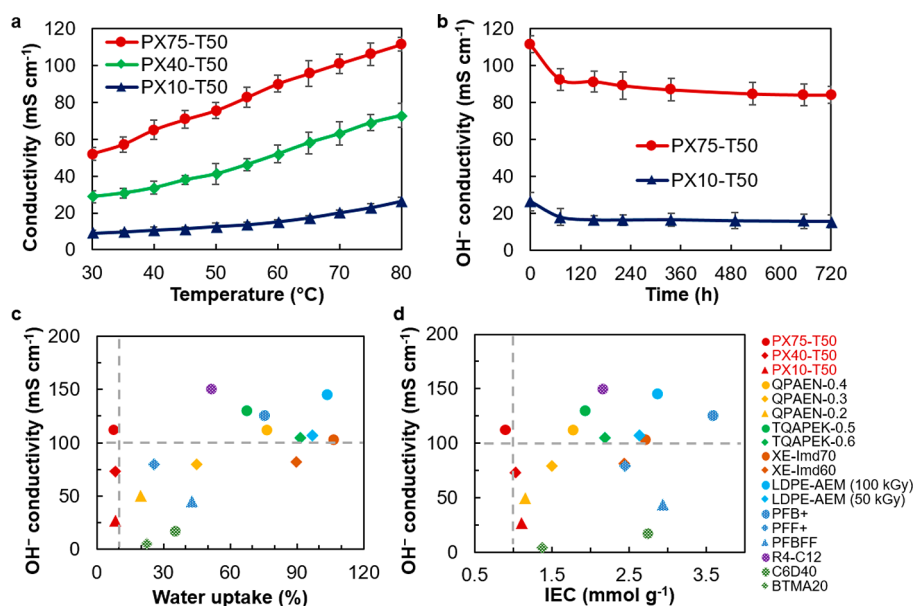


**Figure 3.** Hydroxide conductivity of pyrazolium cross-linked poly(triptycene ether sulfone) membranes. (a) Temperature-dependent conductivity of samples. (b) OH<sup>-</sup> conductivity of PX75-T50 and PX10-T50 in 1 M KOH solution at 80 °C. (c) Hydroxide conductivity versus water uptake. Data points at 80 °C were collected to be compared. (d) Hydroxide conductivity versus IEC. Experimental data points at 20 °C were collected to be compared. Legends for (c) and (d) are in (d). References for data points in (c) and (d): QPAEN,<sup>31</sup> TQAPEK,<sup>32</sup> XE-Imd,<sup>11</sup> LDPE-AEM,<sup>33</sup> PF,<sup>34</sup> R4-C12,<sup>35</sup> and C6D40 and BTMA20.<sup>36</sup> For all experiments, mean values from triplicate experiments are used unless otherwise noted.

## IONIC CROSS-LINKS REDUCE WATER UPTAKE BUT ENHANCE OH<sup>-</sup> CONDUCTIVITY

Hydroxide conductivity over a temperature range of 30–80 °C, measured every 5 °C, reveals that PX75-T50 achieved 95.7 and 101.2 mS cm<sup>-1</sup> at 65 and 70 °C (Figure 3a). A conductivity of  $\approx 100$  mS cm<sup>-1</sup> at a working temperature of fuel cells (generally 60–80 °C) satisfies the standards of U.S. Department of Energy for reliable operation. PX75-T50 showed a conductivity of 52.1 mS cm<sup>-1</sup> at 30 °C, and PX40-T50 and PX10-T50 showed progressively lower values of 28.8 and 9.0 mS cm<sup>-1</sup> at the same temperature. At 80 °C, PX75-T50, PX40-T50, and PX10-T50 showed conductivities of 111.6, 73.1, and 26.5 mS cm<sup>-1</sup>, respectively. Activation energies ( $E_a$ ) calculated from conductivity data using an Arrhenius equation (Figure S17) show the highly cross-linked membrane, PX75-T50, to have lower  $E_a$  of 13.7 kJ mol<sup>-1</sup> than those of PX40-T50 and PX10-T50, which are, respectively, 17.6 and 18.9 kJ mol<sup>-1</sup>. Low  $E_a$  value for PX75-T50 is attributed to facilitated ion transport along cross-linked ionic highways.

To probe the long-term alkaline stability, membranes were soaked in 1 M KOH solution at 80 °C, and conductivity values were tracked for 720 h. PX75-T50 has an initial conductivity of 111.6 mS cm<sup>-1</sup>, which decreased to 84.3 mS cm<sup>-1</sup> after 720 h, thereby retaining 76% of the initial performance (Figure 3b). The initial decrease is likely due to hydroxide-induced degradation of residual pyrazolium chlorides or nucleophilic cleavage of cross-links activated by stress on the polymer films. PX10-T50 retained 26.5 mS cm<sup>-1</sup>, 61% of its initial value, after the same test conditions. PX75-T50 displayed a slow decrease of conductivity to be plateaued after 532 h and stabilized at 84 mS cm<sup>-1</sup> after 30 days. NMR studies of the model cations (4 and 7) and membrane stability data support two operative degradation mechanisms: cleavage of the ether linkages and deprotonation of alpha protons of the pyrazolium 4-substituents (Figures 2, 3b, S9, and S10). We do recognize

that C–N or C–C bonds may offer additional stability relative to the phenolic C–O bonds, and previous studies have pointed to ether linkages as potentially having limited alkaline stability (see Figures S9 and S10 and Note S1 on the use of polyarylether and alkaline stability).<sup>8,11,32,33,37</sup> It is important to note that the ether linkages in the polymer main chain are also a potential point of reactivity.

Highly cross-linked membranes are mechanically resistive to water uptake (swelling). Our cross-linked membranes display low water uptakes of less than 10% (Figures 3c and S18a) with values of 7.9, 8.5, and 8.8% at 80 °C observed for PX75-T50, PX40-T50, and PX10-T50, respectively. As expected, the water uptake is inversely correlated to  $m$ , and in accord, swelling ratios of 2.6, 4.3, and 5.8% at 80 °C were observed for PX75-T50, PX40-T50, and PX10-T50, respectively (Figure S18b). As can be seen from data summarized from the literature (Figure 3c), hydroxide conductivity generally increases with water uptake because of the hydration of cationic centers. The literature reports that samples having higher conductivity over 100 mS cm<sup>-1</sup> and water uptake of greater than 50% are common. Excessive water uptake membrane swelling leads to decreased fuel cell output through compromised contact with the two electrodes. Membranes that are highly conductive with minimal water uptake and swelling are desired, and finding systems that do not suffer from reduced conductance at low water uptake levels is rare. In this context, PX75-T50, which has reduced water uptake and the highest conductivity, is a key advancement. The effectiveness of our design is also revealed by IEC analysis. All of our cross-linked membranes have low IECs of 0.91, 1.03, and 1.12 mmol g<sup>-1</sup> for PX75-T50, PX40-T50, and PX10-T50, respectively, but all maintain high conductivity (Figure 3d and Table S3). PX75-T50 has the remarkable property of having conductivity higher than 100 mS cm<sup>-1</sup> with an extremely low IEC of 0.91 mmol g<sup>-1</sup>. Also within our series, it has the highest conductivity and lowest IEC, which supports the concept that the assembly of the

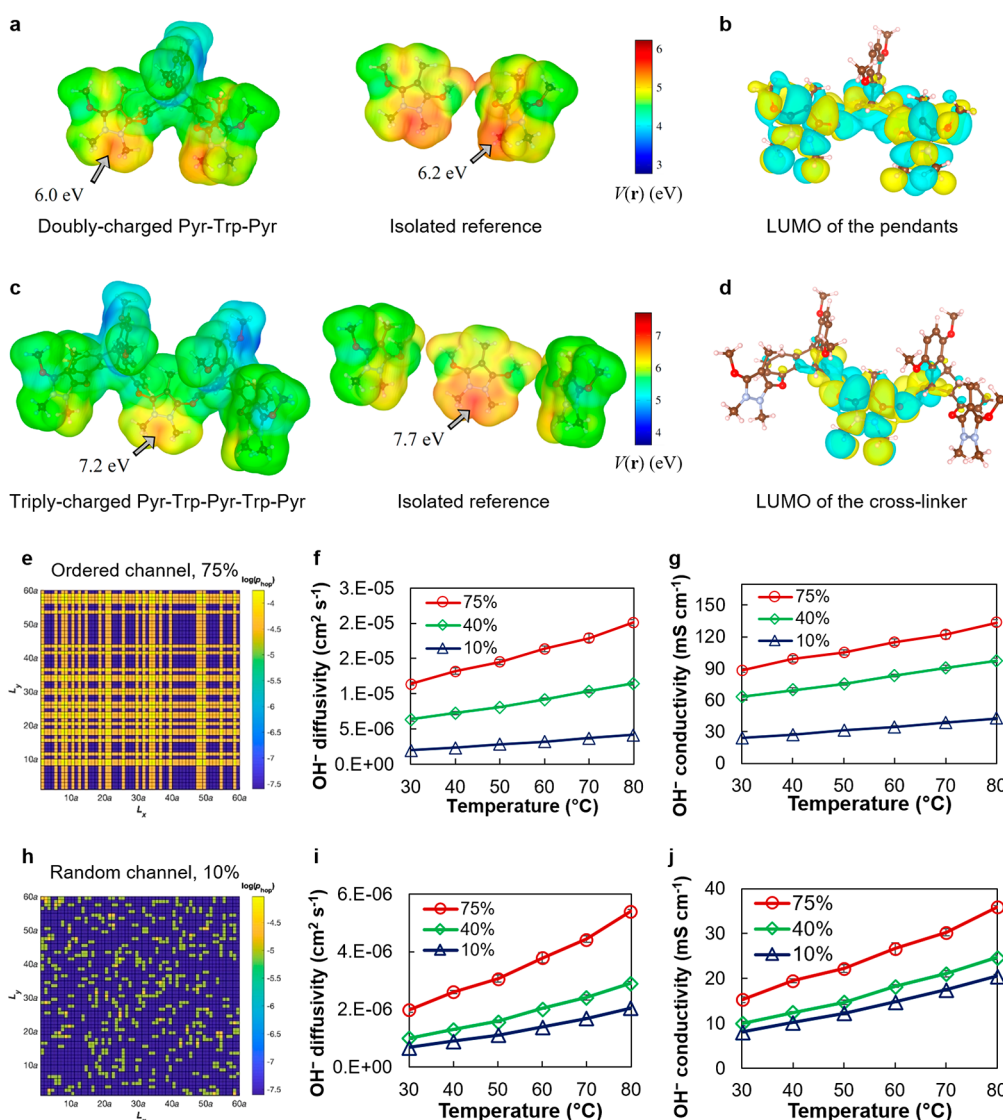


**Figure 4.** Computational studies. (a–d) DFT analysis of charge delocalization in triptycene-connected pyrazolium cations. (a) Electrostatic potential (ESP) mapped on the  $0.01 \text{ e}^{-}\text{\AA}^{-3}$  isodensity surface of model structures where two pyrazoliums (Pyr) are connected to a triptycene (Trp) and the corresponding non-cross-linked reference. (b) LUMO of the chemical structure in (a). (c) ESP mapped on the  $0.01 \text{ e}^{-}\text{\AA}^{-3}$  isodensity surface of model structures where three pyrazoliums and two triptycenes are connected in an alternating way and the corresponding non-cross-linked reference. For (a) and (c), the arrows and associated numbers point at the maximum value of the ESP map, and ESP was projected on an isosurface of the electron density ( $0.01 \text{ e}^{-}\text{\AA}^{-3}$ ). (d) LUMO of the chemical structure in (c). The ends of all methyl or methoxy groups are supposed to have phenyls. However, they were all omitted for the convenience of calculation. See Figure S21 and Files S2–S5 for chemical structures and the ones with coordinates, used in (a–d). (e–j) 2D-LMC studies of ion hopping. (e) Anion hopping probability distribution map for a polymer network constructed by orderly placed cross-linkers for  $m = 75\%$ . (f, g) Calculated  $\text{OH}^{-}$  diffusivity and conductivity at different  $m$  as a function of temperature, respectively. (h) Anion hopping probability distribution map for a polymer network constructed by randomly placed cross-linkers for  $m = 10\%$ . (i, j) Calculated  $\text{OH}^{-}$  diffusivity and conductivity at different  $m$  values as a function of temperature, respectively. Probability maps of the entire cases are in Figure S23 and see SI for details of the calculation.

cations in chains through a combination of cross-linking and grafting creates the facilitated transport we refer to as an ionic highway.

These observations prompted us to investigate the internal sample morphology and structures of the three samples having a different  $m$  linking. X-ray scattering experiments revealed that although the lightly cross-linked membrane, PX10-T50, had structures with  $d$ -spacing of 16.8 nm the more highly cross-linked membranes, PX40-T50 and PX75-T50, displayed featureless scattering patterns (Figure S19). The X-ray scattering data suggest that a high  $m$  may remove nanoscale phase segregations in the membrane. Thermogravimetric

analysis (Figure S20) showed slightly higher char yields with heating to  $1000^\circ\text{C}$  for PX75-T50 of 51% relative to PX40-T50 and PX10-T50 with 49 and 46%, which is also consistent with a higher  $m$ . Overall, achieving the highest conductivity with the lowest water uptake and IEC (Figure 3) demonstrates that the formation of ionic highways is a promising approach for efficient hydroxide transport (Figures 1, 3, and S17).

## COMPUTATIONAL STUDIES ON CHARGE DELOCALIZATION AND IONIC HIGHWAYS

Motivated by these findings, we decided to investigate the microscopic origin of charge transport in ionic highways using

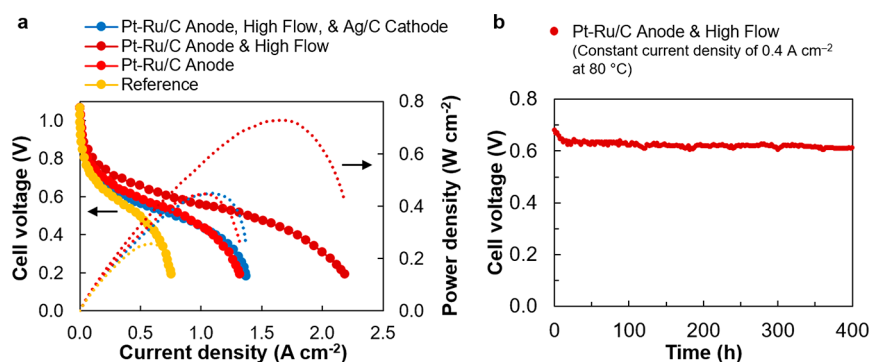


**Figure 5.**  $\text{H}_2/\text{O}_2$  AEMFC performance with PX75-T50. (a) Polarization curves with different catalysts and higher flow rates. Data points with filled circles and dotted lines are for cell voltage and power density, respectively. (b) AEMFC durability test at a constant current density of  $0.4 \text{ A cm}^{-2}$  at  $80^\circ\text{C}$ , with Pt–Ru/C anode, Pt/C cathode, and high gas flow. Reference condition means Pt/C for both electrodes,  $0.2 \text{ L min}^{-1}$  for both gases,  $80^\circ\text{C}$ , 100% RH, and zero backpressure. Besides the reference, the legend contains variables changed compared to the reference. High flow means  $1.0 \text{ L min}^{-1}$  for both gases. Catalyst loading for all electrodes is  $0.5 \text{ mg}$  of metal (or bimetal) per unit  $\text{cm}^2$ .

atomic-scale simulations. We focused first on molecular models of pyrazolium cations cross-linked with triptycene units, which we could compare directly to non-cross-linked structures. An analysis of the electrostatic potential (ESP) of model geometries, which was derived from electronic structure calculations based on DFT, indicates that the connections of the pyrazolium (Pyr) to triptycene (Trp) lead to a significant lowering of the maximum of the electrostatic potential, corresponding to a softening of the charge density (Figure 4a,c, Note S3; Figure S21 for model chemical structures). Compared to the corresponding non-cross-linked control systems, the doubly (Pyr–Trp–Pyr) and triply charged (Pyr–Trp–Pyr–Trp–Pyr) systems, respectively, show a decrease of 0.2 and 0.5 eV of the ESP maximum. Assuming that a hydroxide can be reasonably well approximated as a point charge, this results in weaker hydroxide interactions with the cross-linked cations, which leads to a lowering of the activation energy for the hopping between adjacent cationic sites in our molecular models and improved alkaline stability. Furthermore, the extensively delocalized lowest unoccupied molecular orbital (LUMO) of both doubly charged and triply charged cross-linked systems provides additional evidence of charge delocalization over the basal benzene wings of the triptycene units (Figure 4b,d).

To further investigate the system, we constructed model systems of ionic networks using the 2D lattice Monte Carlo (2D-LMC) model,<sup>38,39</sup> wherein we simulated ionic conductivity in differently formed channels with varying  $m$  (Figure 4e–j, Note S4). We built two systems where conducting channels are orderly or randomly aligned. In the two systems,  $m$  values were changed to be 75, 40, and 10% (Table S1 was used for equivalence of monomers). The probability of hydroxide transport between cross-linked and non-cross-linked sites was determined by the Arrhenius equation, where the activation energies for transport between linked cations and nonlinked cations were extrapolated from our experimental hydroxide conductivity data (see SI for details). Diffusivity and conductivity values were higher in the ordered systems (Figure 4f, g, i, and j). The conductivity from an ordered system with 10% cross-linking was higher than a random system with 75% cross-linking. This observation implies that construction of ionic highways is necessary for the significant improvements in the conductivity of the network. At a lower  $m$ , the cross-links were scattered, making it challenging to form ion transport

pathways (highways) throughout the entire polymer network. At the same time, a higher  $m$  formed longer cross-linked path lengths, which should significantly boost the global diffusion of the anions. The conductivities predicted by the 2D-LMC model are in good agreement with the experimental measurements, capturing both the positive correlations between conductivity and  $m$  and the Arrhenius dependence of conductivity on temperature (Figure 4g, j, and Figure S22 and S25). The fact that the ordered channel model gives a more accurate prediction for  $m = 75\%$  and the random channel model gives an accurate prediction for  $m = 10\%$  reveals the nature of our membranes at different degrees of cross-linking.

## FUEL CELL PERFORMANCE

Membrane electrode assemblies using PX75-T50 demonstrated high power density and stability, generating typical polarization curves that include an activation region, an Ohmic region, and a mass transport region (Figures 5a and S26). AEMFC performance progressively improved by changing catalyst for the anode and increasing gas flow rate. A reference condition (Pt/C,  $0.5 \text{ mg}_{\text{Pt}} \text{ cm}^{-2}$ , for both electrodes, flow rate of  $0.2 \text{ L min}^{-1}$  for both gases,  $80^\circ\text{C}$ , 100% RH, and zero backpressure) enabled a peak power density of  $0.26 \text{ W cm}^{-2}$  at  $0.59 \text{ A cm}^{-2}$  (Figure 5a), which is comparable to benchmark systems at the same working conditions.<sup>6,11,40</sup> Changing the anode catalyst to Pt–Ru/C ( $0.5 \text{ mg}_{\text{Pt}} \text{ cm}^{-2}$  and  $0.25 \text{ mg}_{\text{Ru}} \text{ cm}^{-2}$ ) increased the peak power density to  $0.45 \text{ W cm}^{-2}$ . Increasing gas flow rate to  $1.0 \text{ L min}^{-1}$  for both gases, while keeping Pt–Ru/C for the anode, further increased the peak power density to  $0.73 \text{ W cm}^{-2}$ . As can be seen from previous studies, more active catalysts reduce activation barriers for the hydrogen oxidation reaction, and faster gas transport gives higher rates (Figure S27).<sup>6,33</sup> We also demonstrated that the fuel cells with PX75-T50 give high performance with more economical silver catalysts. Ag/C,  $0.5 \text{ mg}_{\text{Ag}} \text{ cm}^{-2}$ , on cathode resulted in  $0.47 \text{ W cm}^{-2}$  peak power density, with Pt–Ru/C for the anode and the high flow rate. Although a greater voltage drop was observed from the polarization curve with the Ag/C cathode, this is a promising result considering substantial power output and significantly lower price of silver (the price of Ag is  $\approx 2\%$  of that of Pt).

To test single-cell durability, a constant current discharge of  $0.40 \text{ A cm}^{-2}$  was applied at  $80^\circ\text{C}$ , for 400 h under the conditions used for “Pt–Ru/C Anode & High Flow”. Although



there is some initial loss, only a 10% voltage decrease was observed (Figure 5b) over this entire test. This reliable long-term cell operation is consistent with the membrane stability data (Figure 3b), and the mechanical stability of the membrane. PX75-T50 displays only 8% water uptake and 3% swelling ratio at 80 °C. This improved mechanical stability, as compared to the previous reports,<sup>7,11,13</sup> results in reliable long-term operation by maintaining conformal contact between the membrane and the electrode assembly.

## CONCLUSIONS AND OUTLOOK

We synthesized a new generation of AEMs from pyrazolium cross-linked triptycene copolymers, wherein charges are delocalized to construct ionic highways for lower conduction barriers and increased chemical/mechanical stability. The membranes achieve enhanced properties with decreased water uptake and lower IEC, features that diverge from the present trends among AEMs. These rare features are the result of ionic highway networks that are formed from the unique cross-linked structures in the membranes. Computational studies on ESP and 2D-LMC reveal how extended networks of pyrazolium and triptycene produce ionic highways by lowering diffusion barriers. The peak power density of 0.73 W cm<sup>-2</sup> from platinum-group-metal electrodes, 0.47 W cm<sup>-2</sup> from the silver-based cathode, and stable long-term cell operation make the materials further qualify this approach as promising. The concept of assembling an ionic highway using charge-delocalized cations as cross-linkers is herewith established to develop new generations of high performing AEMs for cleaner energy generation.

## ASSOCIATED CONTENT

### Supporting Information

The Supporting Information is available free of charge on the ACS Publications website at DOI: 10.1021/jacs.9b08749.

Details about materials, characterization methods, synthetic procedures, characterization data, and computational studies (PDF)

Calculated structure for 4-methyl-3,5-diphenoxy-1,2-diphenyl-pyrazolium without H<sup>+</sup> (XYZ)

Calculated structure for doubly-charged (Pyr-Trp-Pyr) (XYZ)

Calculated structure for triply-charged (Pyr-Trp-Pyr-Trp-Pyr) (XYZ)

Calculated structure for non-cross-linked control system of the doubly-charged (Pyr-Trp-Pyr) (XYZ)

Calculated structure for non-cross-linked control system of the triply-charged (Pyr-Trp-Pyr-Trp-Pyr) (XYZ)

## AUTHOR INFORMATION

### Corresponding Authors

\*E-mail: jcg@mit.edu.

\*E-mail: tsuager@mit.edu.

### ORCID

Yoonseob Kim: 0000-0002-6892-8281

Yanming Wang: 0000-0002-0912-681X

Arthur France-Lanord: 0000-0003-0586-1945

You-Chi Mason Wu: 0000-0002-6585-7908

Sibo Lin: 0000-0001-5922-6694

Jeffrey C. Grossman: 0000-0003-1281-2359

Timothy M. Swager: 0000-0002-3577-0510

## Author Contributions

<sup>†</sup>Y.W. and A.F.-L. contributed equally.

## Notes

The authors declare no competing financial interest.

## ACKNOWLEDGMENTS

This work was supported by a seed grant from the MIT Energy Initiative. Yanming W. and A.F.-L. acknowledge the Toyota Research Institute (TRI), the Extreme Science and Engineering Discovery Environment, supported by the National Science Foundation grant number ACI-1053575, and the National Energy Research Scientific Computing Center, a DOE Office of Science User Facility supported by the Office of Science of the U.S. Department of Energy under Contract No. DE-AC02-05CH11231, for providing computational support.

## REFERENCES

- (1) Cano, Z. P.; Banham, D.; Ye, S.; Hintennach, A.; Lu, J.; Fowler, M.; Chen, Z. Batteries and Fuel Cells for Emerging Electric Vehicle Markets. *Nat. Energy* **2018**, 3 (4), 279–289.
- (2) Shao, Y.; Yin, G.; Wang, Z.; Gao, Y. Proton Exchange Membrane Fuel Cell from Low Temperature to High Temperature: Material Challenges. *Journal of Power Sources*; Elsevier, 2007; pp 235–242.
- (3) Hickner, M. A.; Herring, A. M.; Coughlin, E. B. Anion Exchange Membranes: Current Status and Moving Forward. *Journal of Polymer Science, Part B: Polymer Physics*; John Wiley & Sons, Ltd., 2013; pp 1727–1735.
- (4) Ran, J.; Wu, L.; He, Y.; Yang, Z.; Wang, Y.; Jiang, C.; Ge, L.; Bakangura, E.; Xu, T. Ion Exchange Membranes: New Developments and Applications. *J. Membr. Sci.* **2017**, 522, 267–291.
- (5) Gottesfeld, S.; Dekel, D. R.; Page, M.; Bae, C.; Yan, Y.; Zelenay, P.; Kim, Y. S. Anion Exchange Membrane Fuel Cells: Current Status and Remaining Challenges. *J. Power Sources* **2018**, 375, 170–184.
- (6) Maurya, S.; Fujimoto, C. H.; Hibbs, M. R.; Narvaez Villarrubia, C.; Kim, Y. S. Toward Improved Alkaline Membrane Fuel Cell Performance Using Quaternized Aryl-Ether Free Polyaromatics. *Chem. Mater.* **2018**, 30 (7), 2188–2192.
- (7) Wang, J.; Zhao, Y.; Setzler, B. P.; Rojas-Carbonell, S.; Ben Yehuda, C.; Amel, A.; Page, M.; Wang, L.; Hu, K.; Shi, L.; et al. Poly(Aryl Piperidinium) Membranes and Ionomers for Hydroxide Exchange Membrane Fuel Cells. *Nat. Energy* **2019**, 4, 392–398.
- (8) Hossain, M. M.; Hou, J.; Wu, L.; Ge, Q.; Liang, X.; Mondal, A. N.; Xu, T. Anion Exchange Membranes with Clusters of Alkyl Ammonium Group for Mitigating Water Swelling but Not Ionic Conductivity. *J. Membr. Sci.* **2018**, 550, 101–109.
- (9) Arges, C. G.; Ramani, V. Two-Dimensional NMR Spectroscopy Reveals Cation-Triggered Backbone Degradation in Polysulfone-Based Anion Exchange Membranes. *Proc. Natl. Acad. Sci. U. S. A.* **2013**, 110 (7), 2490–2495.
- (10) Dekel, D. R. Review of Cell Performance in Anion Exchange Membrane Fuel Cells. *J. Power Sources* **2018**, 375, 158–169.
- (11) Lee, K. H.; Cho, D. H.; Kim, Y. M.; Moon, S. J.; Seong, J. G.; Shin, D. W.; Sohn, J. Y.; Kim, J. F.; Lee, Y. M. Highly Conductive and Durable Poly(Arylene Ether Sulfone) Anion Exchange Membrane with End-Group Cross-Linking. *Energy Environ. Sci.* **2017**, 10 (1), 275–285.
- (12) Hu, E. N.; Lin, C. X.; Liu, F. H.; Yang, Q.; Li, L.; Zhang, Q. G.; Zhu, A. M.; Liu, Q. L. Cross-Linked Poly(Vinylbenzyl Chloride) Anion Exchange Membranes with Long Flexible Multihead for Fuel Cells. *ACS Appl. Energy Mater.* **2018**, 1 (7), 3479–3487.
- (13) Wang, L.; Peng, X.; Mustain, W. E.; Varcoe, J. R. Radiation-Grafted Anion-Exchange Membranes: The Switch from Low- to High-Density Polyethylene Leads to Remarkably Enhanced Fuel Cell Performance. *Energy Environ. Sci.* **2019**, 12, 1575–1579.
- (14) Shin, D. W.; Guiver, M. D.; Lee, Y. M. Hydrocarbon-Based Polymer Electrolyte Membranes: Importance of Morphology on Ion

Transport and Membrane Stability. *Chemical Reviews*; American Chemical Society, 2017; pp 4759–4805.

(15) Kawasumi, K.; Wu, T.; Zhu, T.; Chae, H. S.; Van Voorhis, T.; Baldo, M. A.; Swager, T. M. Thermally Activated Delayed Fluorescence Materials Based on Homoconjugation Effect of Donor-Acceptor Triptycenes. *J. Am. Chem. Soc.* **2015**, *137* (37), 11908–11911.

(16) Hugar, K. M.; Kostalik, H. A.; Coates, G. W. Imidazolium Cations with Exceptional Alkaline Stability: A Systematic Study of Structure-Stability Relationships. *J. Am. Chem. Soc.* **2015**, *137* (27), 8730–8737.

(17) de Paul Nzuwah Nziko, V.; Shih, J.-L.; Jansone-Popova, S.; Bryantsev, V. S. Quantum Chemical Prediction of PK a Values of Cationic Ion-Exchange Groups in Polymer Electrolyte Membranes. *J. Phys. Chem. C* **2018**, *122*, 2490–2501.

(18) Kim, D. S.; Fujimoto, C. H.; Hibbs, M. R.; Labouriau, A.; Choe, Y. K.; Kim, Y. S. Resonance Stabilized Perfluorinated Ionomers for Alkaline Membrane Fuel Cells. *Macromolecules* **2013**, *46* (19), 7826–7833.

(19) Swager, T. M. The Molecular Wire Approach to Sensory Signal Amplification. *Acc. Chem. Res.* **1998**, *31* (5), 201–207.

(20) Mohanty, A. D.; Bae, C. Mechanistic Analysis of Ammonium Cation Stability for Alkaline Exchange Membrane Fuel Cells. *J. Mater. Chem. A* **2014**, *2* (41), 17314–17320.

(21) Hugar, K. M.; You, W.; Coates, G. W. Protocol for the Quantitative Assessment of Organic Cation Stability for Polymer Electrolytes. *ACS Energy Lett.* **2019**, *4* (7), 1681–1686.

(22) Fernández, I.; Dyker, C. A.; DeHope, A.; Donnadieu, B.; Frenking, G.; Bertrand, G. Exocyclic Delocalization at the Expense of Aromaticity in 3,5-Bis( $\pi$ -Donor) Substituted Pyrazolium Ions and Corresponding Cyclic Bent Allenes. *J. Am. Chem. Soc.* **2009**, *131* (33), 11875–11881.

(23) Pan, J.; Chen, C.; Li, Y.; Wang, L.; Tan, L.; Li, G.; Tang, X.; Xiao, L.; Lu, J.; Zhuang, L. Constructing Ionic Highway in Alkaline Polymer Electrolytes. *Energy Environ. Sci.* **2014**, *7* (1), 354–360.

(24) Ge, Q.; Ran, J.; Miao, J.; Yang, Z.; Xu, T. Click Chemistry Finds Its Way in Constructing an Ionic Highway in Anion-Exchange Membrane. *ACS Appl. Mater. Interfaces* **2015**, *7* (S1), 28545–28553.

(25) Lavallo, V.; Dyker, C. A.; Donnadieu, B.; Bertrand, G. Synthesis and Ligand Properties of Stable Five-Membered-Ring Allenes Containing Only Second-Row Elements. *Angew. Chem.* **2008**, *120* (29), 5491–5494.

(26) Fan, J.; Willdorf-Cohen, S.; Schibli, E. M.; Paula, Z.; Li, W.; Skalski, T. J. G.; Sergeenko, A. T.; Hohenadel, A.; Frisken, B. J.; Magliocca, E.; Mustain, W. E.; Diesendruck, C. E.; Dekel, D. R.; Holdcroft, S. Poly(Bis-Arylimidazoliums) Possessing High Hydroxide Ion Exchange Capacity and High Alkaline Stability. *Nat. Commun.* **2019**, *10*, 2306.

(27) Kim, Y.; Moh, L. C. H.; Swager, T. M. Anion Exchange Membranes: Enhancement by Addition of Unfunctionalized Triptycene Poly(Ether Sulfone)s. *ACS Appl. Mater. Interfaces* **2017**, *9* (49), 42409–42414.

(28) Moh, L. C. H.; Goods, J. B.; Kim, Y.; Swager, T. M. Free Volume Enhanced Proton Exchange Membranes from Sulfonated Triptycene Poly(Ether Ketone). *J. Membr. Sci.* **2018**, *549*, 236–243.

(29) Li, Y.; Cao, R.; Lippard, S. J. Design and Synthesis of a Novel Triptycene-Based Ligand for Modeling Carboxylate-Bridged Diiron Enzyme Active Sites. *Org. Lett.* **2011**, *13* (19), 5052–5055.

(30) Navale, T. S.; Rathore, R. A Practical Synthesis of 1,4,5,8-Tetramethoxyanthracene from Inexpensive and Readily Available 1,8-Dihydroxyanthraquinone. *Synthesis* **2012**, *44* (5), 805–809.

(31) Hu, E. N.; Lin, C. X.; Liu, F. H.; Wang, X. Q.; Zhang, Q. G.; Zhu, A. M.; Liu, Q. L. Poly(Arylene Ether Nitrile) Anion Exchange Membranes with Dense Flexible Ionic Side Chain for Fuel Cells. *J. Membr. Sci.* **2018**, *550*, 254–265.

(32) Li, L.; Wang, X. Q.; Zhu, A. M.; Lin, C. X.; Yang, Q.; Liu, Q. L.; Zhang, Q. G. Highly Conductive Anion Exchange Membranes with Long Flexible Multication Spacer. *J. Membr. Sci.* **2018**, *553*, 209–217.

(33) Wang, L.; Brink, J. J.; Liu, Y.; Herring, A. M.; Ponce-González, J.; Whelligan, D. K.; Varcoe, J. R. Non-Fluorinated Pre-Irradiation-Grafted (Peroxidated) LDPE-Based Anion-Exchange Membranes with High Performance and Stability. *Energy Environ. Sci.* **2017**, *10* (10), 2154–2167.

(34) Lee, W. H.; Mohanty, A. D.; Bae, C. Fluorene-Based Hydroxide Ion Conducting Polymers for Chemically Stable Anion Exchange Membrane Fuel Cells. *ACS Macro Lett.* **2015**, *4* (4), 453–457.

(35) Ran, J.; Wu, L.; Wei, B.; Chen, Y.; Xu, T. Simultaneous Enhancements of Conductivity and Stability for Anion Exchange Membranes (AEMs) through Precise Structure Design. *Sci. Rep.* **2015**, *4*, 6486.

(36) Li, N.; Leng, Y.; Hickner, M. A.; Wang, C. Y. Highly Stable, Anion Conductive, Comb-Shaped Copolymers for Alkaline Fuel Cells. *J. Am. Chem. Soc.* **2013**, *135* (27), 10124–10133.

(37) Liu, L.; Chu, X.; Liao, J.; Huang, Y.; Li, Y.; Ge, Z.; Hickner, M. A.; Li, N. Tuning the Properties of Poly(2,6-Dimethyl-1,4-Phenylene Oxide) Anion Exchange Membranes and Their Performance in H<sub>2</sub>/O<sub>2</sub> Fuel Cells. *Energy Environ. Sci.* **2018**, *11* (2), 435–446.

(38) Avramov, I.; Milchev, A.; Argyrakis, P. Diffusion in a Random Medium: A Monte Carlo Study. *Phys. Rev. E: Stat. Phys., Plasmas, Fluids, Relat. Interdiscip. Top.* **1993**, *47* (4), 2303–2307.

(39) Jacoboni, C.; Reggiani, L. The Monte Carlo Method for the Solution of Charge Transport in Semiconductors with Applications to Covalent Materials. *Rev. Mod. Phys.* **1983**, *55* (3), 645–705.

(40) Wang, X. Q.; Lin, C. X.; Liu, F. H.; Li, L.; Yang, Q.; Zhang, Q. G.; Zhu, A. M.; Liu, Q. L. Alkali-Stable Partially Fluorinated Poly(Arylene Ether) Anion Exchange Membranes with a Claw-Type Head for Fuel Cells. *J. Mater. Chem. A* **2018**, *6* (26), 12455–12465.